

Si-Ge based vertical tunnel field-effect transistor of junction-less structure with improved sensitivity using dielectric modulation for biosensing applications

Lucky Agarwal, Varun Mishra, Ravi Prakash Dwivedi, Vishal Goyal, and Shweta Tripathi
Citation: Chin. Phys. B, 2023, 32 (**12**): 128701. DOI: 10.1088/1674-1056/acc7f6
Journal homepage: http://cpb.iphy.ac.cn; http://iopscience.iop.org/cpb

What follows is a list of articles you may be interested in

Combination of density-clustering and supervised classification for event identification in single-molecule force spectroscopy data

Yongyi Yuan(袁泳怡), Jialun Liang(梁嘉伦), Chuang Tan(谭创), Xueying Yang(杨雪滢), Dongni Yang(杨东尼), and Jie Ma(马杰)
Chin. Phys. B, 2023, 32 (**10**): 108702. DOI: 10.1088/1674-1056/acf03e

Single-molecular methodologies for the physical biology of protein machines

Shuang Wang(王爽), Ying Lu(陆颖), and Ming Li(李明)
Chin. Phys. B, 2022, 31 (**12**): 128702. DOI: 10.1088/1674-1056/ac98a2

Structure-based simulations complemented by conventional all-atom simulations to provide new insights into the folding dynamics of human telomeric G-quadruplex

Yun-Qiang Bian(边运强), Feng Song(宋峰), Zan-Xia Cao(曹赞霞), Jia-Feng Yu(于家峰), and Ji-Hua Wang(王吉华)
Chin. Phys. B, 2021, 30 (**7**): 078702. DOI: 10.1088/1674-1056/abe1a7

Enhancements of the Gaussian network model in describing nucleotide residue fluctuations for RNA

Wen-Jing Wang(王文静) and Ji-Guo Su(苏计国)
Chin. Phys. B, 2021, 30 (**5**): 058701. DOI: 10.1088/1674-1056/abe1a5

Mechano-chemical selections of two competitive unfolding pathways of a single DNA i-motif

Xu Yue (徐悦), Chen Hu (陈虎), Qu Yu-Jie (璩玉杰), Artem K. Efremov, Li Ming (黎明), Ouyang Zhong-Can(欧阳钟灿) , Liu Dong-Sheng(刘冬生), Yan Jie (严洁)
Chin. Phys. B, 2014, 23 (**6**): 068702. DOI: 10.1088/1674-1056/23/6/068702

Si–Ge based vertical tunnel field-effect transistor of junction-less structure with improved sensitivity using dielectric modulation for biosensing applications

Lucky Agarwal[1], Varun Mishra[2], Ravi Prakash Dwivedi[1,†], Vishal Goyal[3], and Shweta Tripathi[4]

[1] *School of Electronics Engineering, Vellore Institute of Technology, Chennai* 600127, *India*
[2] *Department of Electronics and Communication Engineering Graphic Era (deemed to be University), Dehradun, Uttarakhand* 248002, *India*
[3] *Department of Electronics and Communication Engineering, GLA University, Mathura* 281406, *India*
[4] *Department of Electronics and Communication Engineering, Motilal Nehru National Institute of Technology, Allahabad* 211004, *India*

(Received 9 November 2022; revised manuscript received 22 March 2023; accepted manuscript online 28 March 2023)

A dielectric modulation strategy for gate oxide material that enhances the sensing performance of biosensors in junction-less vertical tunnel field effect transistors (TFETs) is reported. The junction-less technique, in which metals with specific work functions are deposited on the source region to modulate the channel conductivity, is used to provide the necessary doping for the proper functioning of the device. TCAD simulation studies of the proposed structure and junction structure have been compared, and showed an enhanced rectification of 10^4 times. The proposed structure is designed to have a nanocavity of length 10 nm on the left- and right-hand sides of the fixed gate dielectric, which improves the biosensor capture area, and hence the sensitivity. By considering neutral and charged biomolecules with different dielectric constants, TCAD simulation studies were compared for their sensitivities. The off-state current I_{OFF} can be used as a suitable sensing parameter because it has been observed that the proposed sensor exhibits a significant variation in drain current. Additionally, it has been investigated how positively and negatively charged biomolecules affect the drain current and threshold voltage. To explore the device performance when the nanogaps are fully filled, half filled and unevenly filled, extensive TCAD simulations have been run. The proposed TFET structure is further benchmarked to other structures to show its better sensing capabilities.

Keywords: biomolecules, high-*k* dielectric, junction-less, vertical tunnel field effect transistor (TFET)

PACS: 87.14.–g, 77.22.Ch, 85.30.–z, 61.82.Fk **DOI:** 10.1088/1674-1056/acc7f6

1. Introduction

Recently biosensors have become a focus of research as they are relatively cheap, highly sensitive and have a significant part to play in medicine, including in customized treatment and highly sensitive point-of-care disease marker detection.[1–3] Electrical detection of biomolecules using field-effect transistors (FETs) is particularly fascinating due to its label-free nature, scalability and on-chip integration of sensor and measurement systems.[4] Nanostructured FETs have gained importance due to their high electrostatic control and large surface-to-volume ratio. The basic idea is to add receptors to the oxide layer of the semiconductor to convert the FET into a biosensor.[5,6] These receptors act as destinations for the selected biomolecules, which produce effects on the semiconductor due to their charge, thus changing its electrical properties.

The subthreshold region plays a vital role in getting the maximum changes in electrical properties, which puts conventional FETs at a greater disadvantage due to their minimum subthreshold swing (*SS*) of 60 mV·decade^{-1}.[7–9] Such biosensors based on FET devices have less sensitivity and response time, and even when they are scaled these give rise to short-channel effects. This in turn leads to a low on-state/off-state current (I_{ON}/I_{OFF}) ratio and high power consumption due to reverse leakage. These limitations have been somewhat alleviated through the introduction of tunnel FETs (TFETs), which are designed to have a similar assembly process, work even at low powers and have a lower *SS* (below 60 mV·decade^{-1}).[9–11] The better subthreshold behavior of TFETs can be leveraged to create extremely effective biosensors. This stands out because TFETs use a fundamentally distinct current injection process called band-to-band tunnelling (BTBT), which gives rise to protection from random dopant variations.[12–14] This tunnelling mechanism is preferred over diffusion as the barriers are thin enough over a large area for effective tunneling and provide a sufficient density of states on both the transmission and receiving sites to provide energetic locations for carriers. According to reports, FET-based biosensors are broadly applicable to the healthcare sector, pollution monitoring and biological pathogen management.[15–17] FET-based biosensors can inspect environmental biohazards and control viral infections economically. According to several researchers, TFET-based biosensors are a potential technology for achieving significantly enhanced sensitivity and response times compared with existing FET-based biosensors.[18–20] To

†Corresponding author. E-mail: raviprakash.dwivedi@vit.ac.in
© 2023 Chinese Physical Society and IOP Publishing Ltd

increase the sensitivity of these devices in terms of high I_{ON}, modified device structures such as dual metal gate, double or triple gate, pocket doping, etc. have been proposed in the literature. Metal oxide based TFET structures[1,17] are a major consideration of researchers, but heterojunction TFETs are no doubt a better alternative for modern integrated circuit technology. However, due to its ease of fabrication, the vertical TFET (V-TFET) structure has attracted more consideration than other reported TFET structures.[20–22] Furthermore, V-TFETs have fewer trapping difficulties, a lower buffer layer leakage current and are easier for building wrap-gated topologies.[23] Therefore, a device analysis of VTFETs as biosensors could be of great interest to many.

Considering the structures reported in the literature, a junction-less VTFET (VJ-TFET) with a nanocavity embedded for biosensing is proposed in this paper. The sensitivity of the proposed structure is simulated on TCAD software and compared with TFET based biosensors. Analysis of the electrical simulation parameters of the proposed device includes looking at the energy band profile, transfer characteristics, drain current sensitivity, I_{ON}/I_{OFF} ratio and *SS*. In order to obtain the highest I_{ON} and lowest I_{OFF}, the cavity's thickness and length for biomolecule detection are also examined. Further, this research also looks at the effects of both neutral and charged biomarkers. To further comprehend the applicability of these biosensors, non-ideal circumstances such as steric hindrance and uneven probe placements have been researched. Lastly, the proposed VJ-TFET structure is benchmarked to previously published works.

2. Device architecture and simulation methodology

A cross-sectional view of the nanocavity entrenched proposed VJ-TFET structure along with its dimensions is shown in Fig. 1. The width of the device is defined by the *x*-axis and its length by the *y*-axis. The proposed VJ-TFET is a dual metal gate structure with a lower work function metal gate around $\phi_{m1} = 4.7$ eV near the source end and $\phi_{m2} = 5.3$ eV near the drain end. A SiO_2/HfO_2 stacked oxide layer is inserted across the top and bottom ends of channel, replacing the conventional gate oxide. In the VJ-TFET, Si–Ge is used as the channel material. In Si–Ge, 30% Ge has been adopted throughout the analysis. Since, Si–Ge has lower bandgap than Si, tunnelling of electrons at the source channel increases, therefore I_{ON} increases. Moreover, due to the vertical structure, vertical tunnelling along with lateral tunnelling is observed, which may result in an increased I_{ON}. The band diagram of the VJ-TFET in the off and on states is shown in Figs. 2(a) and 2(b) for a high-*k* dielectric material. It can be observed from the figure that the high-*k* material (HfO_2) shows more bending, resulting in higher tunnelling, thereby I_{ON} increases, as shown in Fig. 2(c). To make the proposed device structure junctionless a channel body of length 40 nm and thickness 10 nm is doped with an n-type impurity having a carrier concentration of 5×10^{19} cm^{-3}. To form p^+ pockets, platinum metal contacts with a work function of 5.93 eV are activated as source electrodes. This proves the versatility of the suggested structure and shows that there are no additional doping requirements, which solves the issue of random dopant fluctuation. The detailed parameters used in simulation of the VJ-TFET structure are given in Table 1. Further, to improve the confinement of the biomolecules, nanogaps are etched on both sides of the gate dielectric, as shown in Fig. 1. The electrical characteristics of the device junction can be modulated by biomolecules trapped in the nanocavity. The biosensing process is simulated in an air environment so that better sensitivity can be achieved.

Table 1. Structural parameters used in the simulations.

Device parameter	Value
Gate length	40 nm
Nanocavity length	15 nm
Oxide thickness	1 nm
High-*k* thickness	4 nm
Length of source/drain	35 nm
Source, channel and drain doping	n-type 5×10^{19} cm^{-3}
Source work function	$\Phi_s = 5.93$ eV
Drain work function	$\Phi_d = 4.7$ eV
Length of source/drain	35 nm

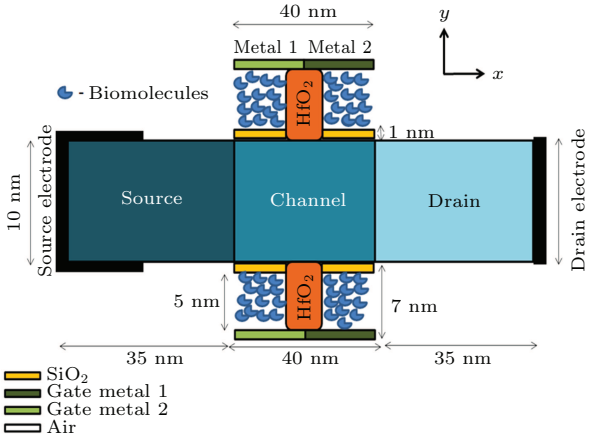


Fig. 1. Cross-sectional view of a VJ-TFET.

The Silvaco ATLAS simulation tool was utilized to run the simulation; it uses the Laplace and Poisson equations to solve the device operation. The device dimensions and other parameters used to simulate the device structure are given in Table 1. Several physical models such as Fermi–Dirac, Shockley–Read–Hall recombination and field-dependent mobility are used to simulate the electrical characteristics of a device.[24] Further, non-local BTBT and quantum models are also advocated to incorporate BTBT and quantum confinement effects, respectively. The two-dimensional VJ-TFET has the same reproduction boundaries and model attributes as a standard VTFET, with the difference that the channel region is

more heavily doped. The proposed structure is calibrated with the experimental data (obtained with the help of the Plot Digitizer tool) of the reported VTFET structure. All the dimensional parameters of the device are kept the same as reported, except for the number of gates.[14] The transfer characteristics calibrated are shown in Fig. 2(d). The results are found to be in good agreement. Further, to make the proposed device work as a sensor, only one type of biomolecule is thought to be immobilized in the nanoedged cavities at any given moment. The permittivity of neutral charged biomolecules ranges from 1 to 10. The effect of varying charged biomolecules based on DNA values reported in the literature[26,27] is also explored at the nanoedged region to test the sensitivity of the proposed structure.

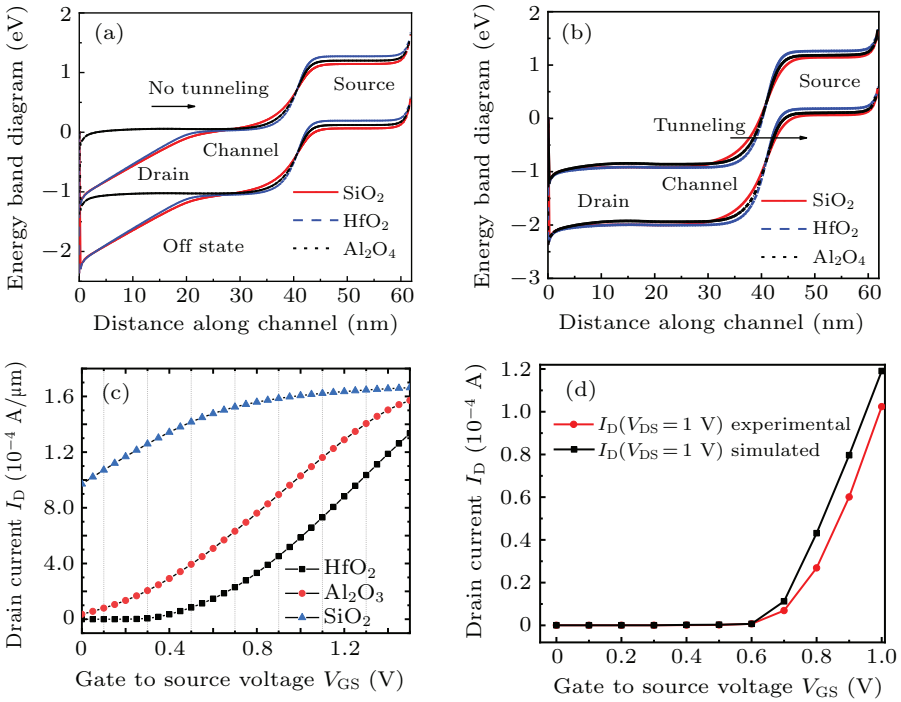


Fig. 2. Energy band diagram of the proposed structure: (a) off state and (b) on state. (c) Calibration of the proposed VTFET structure for dielectric material. (d) Comparison between simulated and experimental data.

2.1. Principle of the proposed VJ-TFET structure

For BTBT, the vertical dual metal double-gate architecture gives superior gate controllability to traditional topologies. The proposed VJ-TFET structure can be used for biosensing applications because of its high I_{ON} and low SS of 33 mV·decade^{-1}, compared with a conventional TFET structure, as observed from Fig. 3. The high I_{ON} may be due to the vertical tunnelling of carriers under a low electric field that reduces phonon scattering, thereby enhancing mobility.[28] An n-channel VJ-TFET structure with molybdenum and iridium as metal gate contacts is analyzed for biomolecule (dielectric constant $k = 1$–10) sensing. Biosensors work by converting the concentrations of various biomolecules into conventional electrical signals utilizing specific physical and chemical reactions. When biomolecules react with the metal surface at the gate contact, a change in gate oxide capacitance occurs, which changes the overall threshold voltage of the device and hence the drain current.

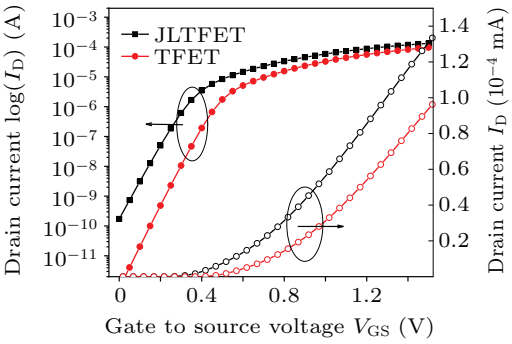


Fig. 3. Comparison of simulated transfer characteristics of the proposed structure with a reference structure.

3. Results and discussion

The findings of simulations of the proposed VJ-TFET based biosensors using different dielectric constants ($k = 1$, 2, 5, 8, 10) are discussed in this section. Further, the effect of diverse neutral, positively and negatively charged biomolecules on current is studied in depth. The value of dielectric constant for the sensing mechanism is selected based on the literature for TFET biosensors.[27,29–31] Lower dielectric constants up to 5 correspond to air, uricase, streptavidin, choline oxidase and (3-aminopropyl)triethoxysilane. Higher dielectric constants correspond to gluten, zein, egg-white lysozyme and acetylene tetrabromide (or 1,1,2,2-tetrabromoethane).

3.1. Effect of neutral biomolecules on the sensitivity of the proposed structure

The variation of the transfer characteristics of neutral biomolecules with different dielectric constants is presented in Fig. 4(a). The drain current when the cavity is filled with air is shown by $k = 1$ in Fig. 4(a). It is clearly evident from the figure that on increasing the dielectric constant, I_{OFF} reduces while I_{ON} remains constant. A high k provides better control over the channel as the oxide capacitance increases, thereby reducing the leakage of charge carriers and increasing the accumulation of charge carriers in the channel region, which enhances I_{ON}. Further, in addition to lateral tunnelling, there is a vertical BTBT in a perpendicular direction to the gate oxide due to the vertical structure that enhanced I_{ON}. Moreover, the use of dual metal architecture in the proposed structure reduced I_{OFF} due to the gate with a higher work function towards the drain end. Therefore, the overall I–V characteristics of the proposed structure are much better than the reported values.

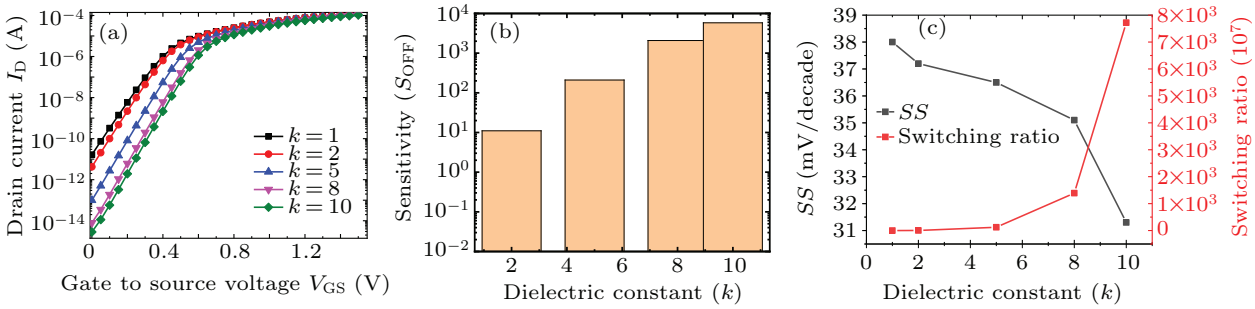


Fig. 4. (a) The I_D–V_{GS} characteristics of biosensors for different dielectric constant values k. (b) Sensitivity of neutral biomolecules for different k. (c) Switching ratio and SS for different k.

Sensitivity is measured in order to analyze the performance of the biosensor. Since it has the capacity to reflect the sensor's response to the sensing targets, the state when the nanogap is empty or filled with air is chosen as a reference. In this work, sensitivity is evaluated with respect to I_{OFF} at fixed V_{DS} as expressed below:[3]

$$S_{OFF} = \frac{I_{OFFair}}{I_{OFFk}}, \tag{1}$$

where I_{OFFair} is the OFF drain current when the etch nanocavity is filled with air and I_{OFFk} signifies the OFF drain current when the etched nanocavity is filled with biomolecules at fixed V_{DS}. The sensitivity of the proposed structure with neutral biomolecules is shown in Fig. 4(b). It is observed from Fig. 4(a) that I_{OFF} reduces on increasing k due to the generation of a large electric field, which improves the sensitivity of the proposed device. However, better sensitivity is obtained for $k = 10$, whose order is of 10^4 as presented in Fig. 4(b). The increase in sensitivity is supported by the decrease in I_{OFF}, because the p^+ source does not produce dominant charge carriers in a junction-less FET device. Further, the increase in sensitivity is supported by Fig. 4(c), which shows the plot of switching ratio and SS against k. It is observed that the switching ratio (I_{ON}/I_{OFF}) and SS improve for higher values of k, which improves the sensitivity of the device.

3.2. Effect of charged biomolecules on sensitivity of the proposed structure

In this section, the impact of positively and negatively charged biomolecules is analyzed in terms of transfer characteristics and sensitivity. Figures 5(a) and 5(b) show the I_D–V_{GS} variation for $k = 2$, considering both positively and negatively charged biomolecules, respectively. The impact of charged biomolecules can be understood in terms of effective gate bias (V_{GSeff}) and flat band voltage (V_{FB}), which can be expressed as[31]

$$V_{GSeff} = V_{GS} - V_{FB}, \tag{2}$$

$$V_{FB} = V'_{FB} - \frac{qN}{C_{eff}}, \tag{3}$$

where V_{GS} is applied gate bias, V_{FB} is the flat band voltage when a charged biomolecule is present, V'_{FB} is the flat band voltage when a charged biomolecule is absent, N is a charged biomolecule and C_{eff} is the effective capacitance. For a positively charged biomolecule, V_{FB} reduces (as observed from Eq. (3), leading to an increase in effective gate bias voltage, which further increases the tunneling of charge carriers due to increase in the surface potential, thereby increasing the drain current. It is clearly evident from Fig. 5(a). that drain current enhances with increase in the value of positively charged biomolecules. This may be due to the decrease in surface potential under the presence of positively charged biomolecules. The range of positively charged biomolecules is from 1×10^{11} C·cm^{-2} to 6×10^{12} C·cm^{-2}. For a fixed V_{GS}, an increase in positively charged biomolecules increases the drain current.

For negatively charged biomolecules V_{FB} increases, suppressing the surface potential and effective gate bias due to which the tunnelling of charge carriers reduces, thereby reducing the drain current. Figure 5(b) shows the variation of I_D–V_{GS} of negatively charged biomolecules for $k = 2$. It is observable from Fig. 5(b) that on increasing the number

of negatively charged biomolecules the drain current is suppressed. Consequently, the electrostatic field also reduces on increasing the number of negatively charged biomolecules due to suppression of V_{GSeff}. The range of negatively charged biomolecules is from -1×10^{11} C·cm^{-2} to -6×10^{12} C·cm^{-2}. Figures 5(c) and 5(d) present the variation of I_{D}–V_{GS} for $k = 5$ considering both positively and negatively charged biomolecules, respectively. For similar reasons to those stated above, the drain current increases with increase in positively charged biomolecules and reduces with negatively charged biomolecules. However, due to the increase in k, I_{OFF} decreases and I_{ON} increases in contrast to the case for $k = 2$. The reason for this can be understood from the expression for C_{eff} in Eq. (3), which shows that for a fixed value of V_{GS} and interface charge, the increase in k will increase or decrease the surface potential as per the polarity of the biomolecule.

Figures 5(e)–5(g) show the transfer characteristics of positively and negatively charged biomolecules for $k = 8$ and $k = 10$, respectively. It is clearly observable that I_{OFF} reduces for higher values of k. The VTFET based biosensor has a reduced ambipolarity effect due to the existence of a dual metal gate with a larger work function on the drain side, that further reduces I_{OFF}. The minimum I_{OFF} of 10^{-18} A is observed in Fig. 5(g) for $k = 10$ and $N = -6\times10^{12}$.

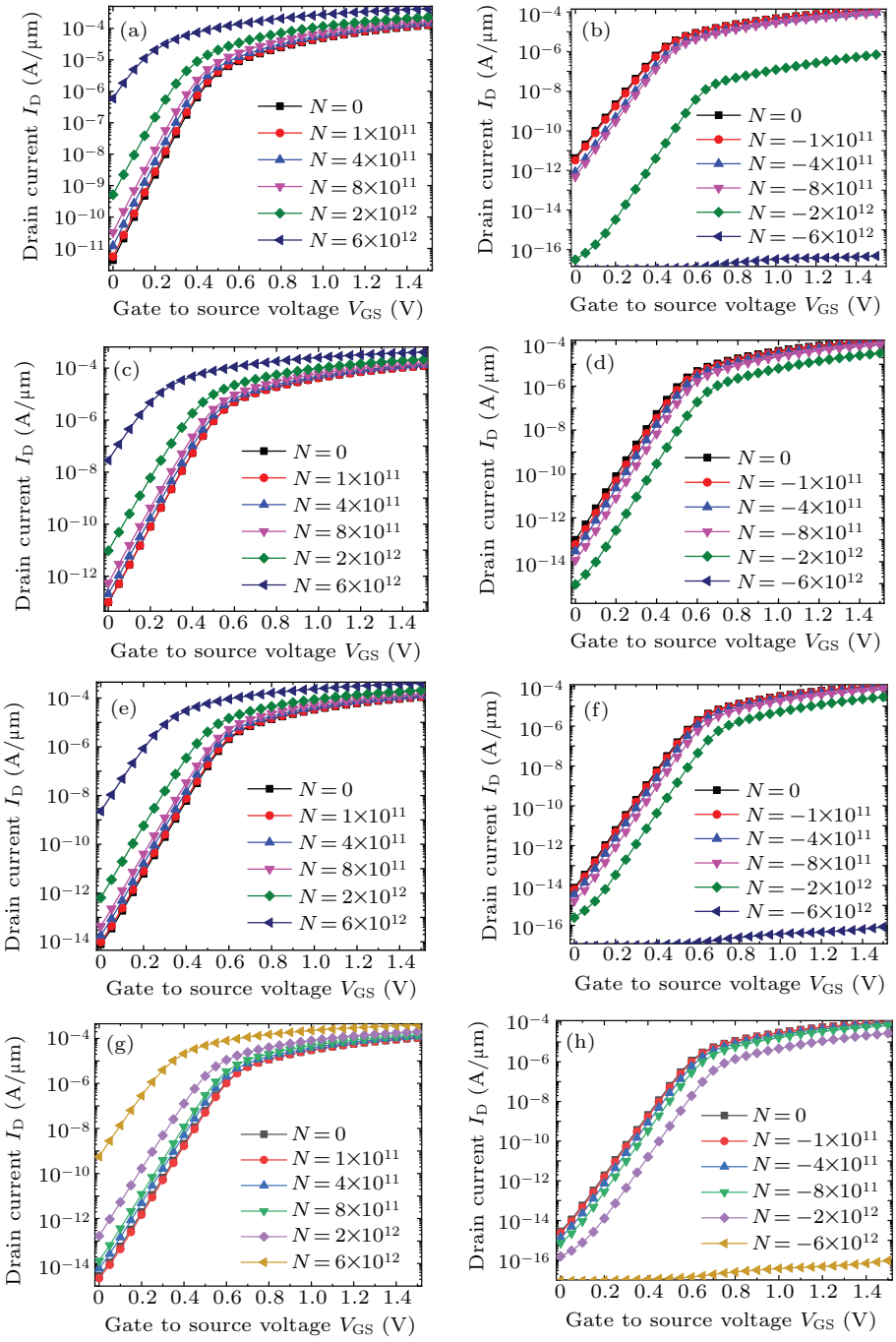


Fig. 5. The I_{D}–V_{GS} characteristics of the proposed biosensor with positive interface charge biomolecules for different dielectric constants k: (a) $k = 2$, (c) $k = 5$, (e) $k = 8$, (g) $k = 10$; and with negative interface charge biomolecules for different k: (b) $k = 2$, (d) $k = 5$, (f) $k = 8$, (h) $k = 10$.

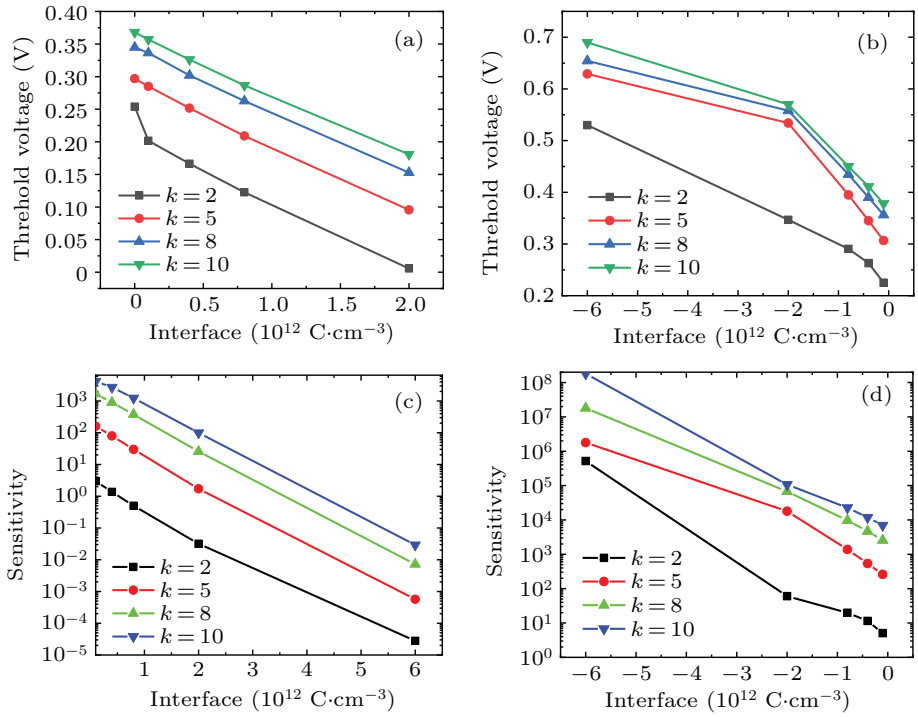


Fig. 6. Threshold voltage variation for different dielectric constants: (a) positively charged biomolecule, (b) negatively charged biomolecule. Sensitivity variation for different dielectric constants: (c) positively charged biomolecule, (d) negatively charged biomolecule.

Furthermore, threshold voltage is plotted with respect to positively and negatively charged biomolecules, as shown in Fig. 6. It is clearly evident from Fig. 6(a) that threshold voltage decreases as the number of positively charged biomolecules increases. The reason behind the decrease in threshold voltage is the reduction in V_{FB} as mentioned in Eq. (3). However, for negatively charged biomolecules the opposite is the case, as observed from Fig. 6(b); i.e., the threshold voltage increases with increase in the number of negatively charged biomolecules due to reduction in the effective gate bias voltage. With the inclusion of the term $-qN/C_{eff}$ in Eq. (3), the effect of negatively charged biomolecules limits the depletion of the p-type channel. As a result, to deplete the channel, a gate voltage greater than the voltage of a neutral biomarker is required; this will increase the threshold voltage with increase in N. Thus, a reduced gate bias voltage would not be sufficient for charge inversion in the channel, thereby increasing the threshold voltage.

Sensitivity is calculated using Eq. (1) and is plotted in Fig. 6(c) with respect to positively and negatively charged biomolecules. It is observable from Fig. 6(c) that sensitivity decreases with the number of positively charged biomolecules; the reason for this is the reduction in V_{FB} which further increases the effective gate bias voltage that enhances I_{OFF}. However, for negatively charged biomolecules, as shown in Fig. 6(d), sensitivity increases with increase in the number of negatively charged biomolecules due to an increase in the depletion width across the channel that increases the threshold voltage of the device. Therefore I_{OFF} decreases, which improves the sensitivity of the device. Furthermore, the transfer characteristic plot for -8×10^{11} cm^{-3} negatively charged biomolecules are given in Fig. 7, which shows a better I_{OFF}. This proves that the junction-less transistor is highly sensitive in terms of I_{OFF}.

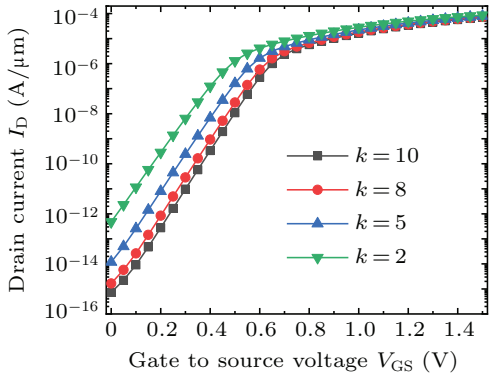


Fig. 7. The I_D–V_{GS} characteristics for negatively charged biomolecules (-8×10^{11} cm^{-3}).

3.3. Effect of irregular fusion of biomolecules in the nanocavity of the proposed structure

All the sensitivity calculations in the previous sections are predicated on the notion that the nanocavities of biosensors are entirely loaded with biomolecules. However, in practice, this assumption is not often fulfilled. When receptors or probes pierce the nanogaps, biomolecules may become immobilized and fuse. It is possible that this hybridization will not continue until all the nanogaps are filled, preventing further biomolecules from entering. This phenomenon is known as steric hindrance, and might lead to a non-uniform step profile

of biomolecules inside the nanogaps. Figure 8 shows the proposed biosensor structure with five different biomolecule hybridization profiles: (a) decreasing steps, (b) increasing steps, (c) non-uniform steps (d) non-ideal hybridization case 1, (e) non-ideal hybridization case 2. For all these distinct nanogap step patterns comparisons are made of their sensitivities.

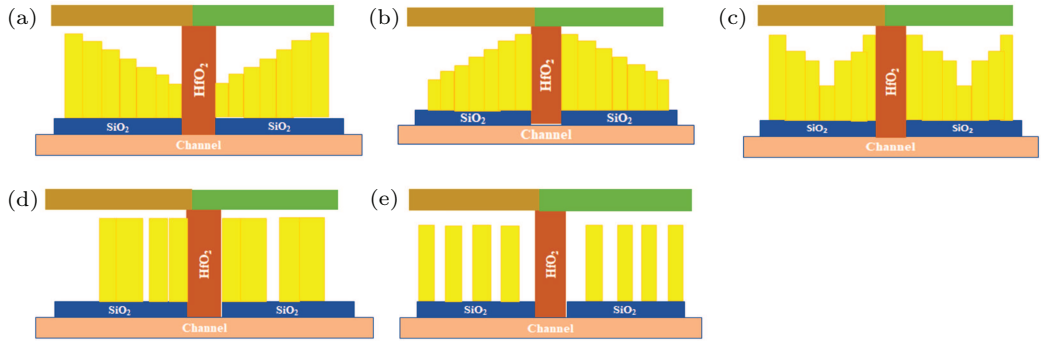


Fig. 8. Different profiles of hybridized nanogaps with (a) increasing step size, (b) decreasing step size, (c) nonuniform step size, (d) non-ideal hybridization case 1, (e) non-ideal hybridization case 2.

To better comprehend how sensitivity is influenced by how much room the biomolecules take up inside the cavities, simulations have been done with fill factors of 40% and 60% for the first three profiles, with $N = -6 \times 10^{12}$ cm^{-3}, $k = 10$, $V_{GS} = 1.5$ V, $V_{DS} = 1$ V. The simulation results for fill factors of 40% and 60% are listed in Table 2. Since the area of the etched nanocavity is 15 nm×5 nm, to maintain a fill factor of 40% the nanocavity is divided into seven equal parts with a cavity width for each cavity of 2.05 nm.[32] For the increasing steps hybridization profile, the step height is taken from 0.2 nm to 2.6 nm with a height difference of 0.4 nm. In the case of the decreasing steps profile, the converse is true. For the non-uniform profile, the step size is taken as 2.6 nm, 1.6 nm, 0.6 nm, 0.2 nm, 0.6 nm, 1.6 nm and 2.6 nm. To maintain a fill factor of 60%, the above same procedure is followed. For all profiles, the width of the steps inside the cavities is similar to the above analysis, while the height is varied from 4.5 nm to 1.5 nm for the increasing steps profile and vice versa for the decreasing steps profile. The height for non-uniform steps is kept at 5 nm, 3.5 nm, 1 nm, 0.5 nm, 1 nm, 3.5 nm and 5 nm. Table 2 shows that the decreasing steps profile has a superior response on average, but the increasing and non-uniform steps profiles have poor sensitivity. This may be due to the electron tunnelling current in the TFET structure at the source–channel junction, which is influenced by the dielectric constant of the gate oxide. Near the tunnelling junction, the decreasing profile has its biggest step, which raises the effective dielectric capacitance around it and hence enhances the sensitivity. Further it can be seen from the data in Table 2 that there is an increment of 8% to 10% in sensitivity when the fill factor is increased from 40% to 60%; this may be due to the increase in gate and channel coupling.

The non-deal hybridization profile depends on the position of the probes.[33] The amount of fusion of biomolecules and probes depends on the position of the probes in the nanocavity, that will in turn influence the sensitivity of the proposed biosensors. Figures 8(d) and 8(e) depict the positions of probes inside cavities for the proposed biosensor structure. The yellow pillar area indicates the presence of biomolecules ($k > 1$), whereas the unshaded area indicates the presence of air ($k = 1$). Considering the position of the probes, two cases (case 1 and case 2) are considered for the study as shown in Figs. 8(d) and 8(e). The data in Table 2 show that when biomolecules are present near the tunnelling junction (case 1) the sensitivity improves, but when biomolecules move away from the junction (case 2) the sensitivity begins to deteriorate, even though the fraction of the area occupied by biomolecules remains constant.

Table 2. Sensitivity comparison for different biomolecule profiles.

Step size profile	Value	
	Fill factor 40%	Fill factor 60%
Increasing	7.6×10^{6}	8.3×10^{6}
Decreasing	5.6×10^{4}	6.1×10^{4}
Non-uniform	9.3×10^{4}	4.6×10^{4}
Case 1	5.3×10^{7}	
Case 2	8.5×10^{6}	

3.4. Standardization of proposed structure with reported work

Dielectric modulated FET and TFET based biosensors have been the subject of several experimental, computer-simulated and analytical modelling investigations. As a result, the sensitivities of other previously published sensors are contrasted with that of the proposed VJ-TFET based biosensor in this section to benchmark the proposed structure.

Table 3 shows the status of the literature. The sensitivities were extracted from the published works and hence the term ‘approximate’ is used in the table. It is evident from Table 3 that the suggested VJ-TFET has superior sensitivity to the other FET based sensors due to the use of low bandgap material and vertical tunnelling, although the published works have different structural, doping and dielectric constant parameters. Numerous biosensor structures have been added to

Table 3 in order to provide an overview of the various types of available biosensors. However, because of the differences in their current injection techniques, TFET-based biosensors have a far higher sensitivity than FET-based biosensors.

Table 3. Comparison of different published FET structures.

Reported biosensor	Sensitivity	ΔA
Junction-less V-TFET (present work)	1.1×10^{8}	2.75×10^{5}
Dual metal Si Ge pocket VTFET[32]	2×10^{6}	0.5×10^{6}
Dual metal Si Ge pocket PNPN TFET[32]	6×10^{3}	1.4×10^{3}
Dual metal PNPN TFET[30]	3×10^{6}	0.75×10^{6}
Dual metal FET[30]	7	1.75
Short gate dual metal TFET[33]	1×10^{6}	2.5×10^{5}
Lateral dual metal TFET[34]	10	2.5
Vertical dual metal TFET[34]	40	4
Dual metal FET[28]	1×10^{4}	2.5×10^{3}
Nanowire TFET[27]	9×10^{3}	2.25×10^{3}
Conventional TFET[27]	50	12.5

Sensitivity of biosensor = $\Delta A\times$ sensitivity of FET based biosensor.
Approximate sensitivity of FET based biosensors is 4.[35]

4. Conclusion

The notion of a dual metal double gate VJ-TFET structure with nanogaps etched at both sides of a fixed dielectric as a highly sensitive biosensor has been presented in this paper. The proposed structure is junction-less with Si–Ge as a channel material; it shows its novelty in terms of ease of fabrication compared with other reported structures. An optimal sensitivity of 1.1×10^{8} is obtained for the proposed structure when fully filled with neutral biomolecules with a dielectric constant of 10. Due to the existence of both lateral and vertical tunnelling, the VJ-TFET has a higher sensitivity. The achieved rectification ratios highlight the proposed structure as a viable option. The effect of charged biomolecules on sensor performance has also been examined. The sensitivity of biosensors is observed to enhance and a value of 2×10^{8} was recorded as negatively charged biomolecules (6×10^{12} C·cm^{-3}) fill the etched nanogap. The utility of the sensor is further examined while accounting for steric impediments and unequal probe positions. The declining partially filled profile and the non-uniform steps profile both demonstrated the highest sensitivity. When the fill factor is increased from 40% to 60%, the sensitivity improves by 8%–10%, indicating that the proposed VJ-TFET is affected by the fill factor. When biomolecules are hybridized away from the tunnelling junction, the sensitivity is more negatively impacted, looking at two distinct possible probe sites. A comparison of the proposed biosensor is made with the MOSFET-based biosensor given in Ref. [35], and is benchmarked against established standards. Hence, the proposed biosensor is a promising candidate for label-free sensing due to its higher sensitivity and lower power consumption.

Acknowledgement

Authors greatly acknowledge MNNIT Allahabad for accessing the software facility.

References

[1] Barbaro M, Bonfiglio A and Raffo L 2006 *IEEE Trans. Electron. Devices* **53** 158
[2] Kim C H, Jung C, Park H G and Choi Y K 2008 *Biochip J.* **2** 127
[3] Chanda M, Das R, Kundu A and Sarkar C K 2017 *Superlattices Microstruct.* **104** 451
[4] Narang R, Saxena M, Gupta R S and Gupta M 2012 *IEEE Electron. Device Lett.* **33** 268
[5] Choi J M, Han J W, Choi S J and Choi Y K 2010 *IEEE Trans. Electron. Devices* **57** 3477
[6] Jayaswal N, Raman A, Kumar N, Singh S 2019 *Superlattices Microstruct.* **125** 256
[7] Singh S, Khosla M and Wadhwa G 2021 *Appl. Phys. A* **127** 16
[8] Tsukada K, Kariya M, Yamaguchi T, Kiwa T, Yamada H, Maehara T, Yamamoto T, Kunitsugu S 2010 *Jpn. J. Appl. Phys.* **49** 024206
[9] Wei W, Lü W, Han Y, Zhang C and Chen D 2023 *Chin. Phys. B* **32** 097301
[10] Gnudi A, Reggiani S, Gnani E and Baccarani G 2012 *IEEE Electron Device Lett.* **33** 336
[11] Li W and Woo J 2020 *IEEE Trans. Electron Device* **67** 1480
[12] Ko E, Lee H, Park J and Shin C 2016 *IEEE Trans. Electron Devices* **63** 5030
[13] Wang B, Hu S and Feng Y 2020 *Chin. Phys. B* **29** 107401
[14] Nigam K, Kondekar P and Sharma D 2016 *Micro Nano Lett.* **11** 319
[15] Choi K M and Choi W Y 2013 *IEEE Electron Device Lett.* **34** 942
[16] Zhang W H, Li Z C, Guan Y H and Zhang Y F 2017 *Chin. Phys. B* **26** 078502
[17] Shan C, Wang Y and Bao M T 2016 *IEEE Trans. Electron. Devices* **63** 2275
[18] Busse S, Scheumann V, Menges B and Mittler S 2002 *Biosensors Bioelectron.* **17** 710
[19] Bhattacharyya A, Chanda M and De D 2019 *IEEE Trans. Electron. Devices* **66** 3988
[20] Bibi F, Villain M, Guillaume C, Sorli B and Gontard N 2016 *Sensors* **16** 1232
[21] Choi W Y, Park B, Lee J D and Liu T K 2007 *IEEE Trans. Electron. Device Lett.* **28** 743
[22] Bhuwalka K K, Sedlmaier S, Ludsteck A K, Toksdorf C and Schulze- and J, Eisele I 2004 *IEEE Trans. Electron. Device* **51** 279
[23] Wirths S, Tiedemann A T, rellenkamp S, Buca D, Zhao Q T and Mantl S 2015 in *Proc. Int. Electron. Devices Meeting* 608
[24] Huang Q, Huang R, Wu C, Zhu H, Chen C, Wang J, Guo L, Wang R, Ye L and Wang Y 2014 *in Proc. IEEE Int. Electron. Devices Meeting* 13
[25] Zhou G, Li R, Vasen T, Qi M, Chae S, Lu Y, Zhang Q, Zhu H, Kuo J M, Kosel T and Wistey M 2012 *in Proc. Int. Electron. Devices Meeting* 32
[26] Devi W V and Bhowmick B 2019 *Micro Nano Lett.* **14** 69
[27] Sarkar D and Banerjee K 2012 *Appl. Phys. Lett.* **100** 143108
[28] Im H, Huang X J, Gu B and Choi Y K 2007 *Nat. Nanotechnol.* **2** 430
[29] Kanungo S, Chattopadhyay S, Gupta P S and Rahaman H 2015 *IEEE Trans. Electron. Devices* **62** 994
[30] Narang R, Saxena M, Gupta R S and Gupta M 2015 *IEEE Trans. Nanotechnol.* **14** 427
[31] Mishra V, Verma Y K and Gupta S K 2019 *Journal of Nanoelectronics and Optoelectronics* **14** 161
[32] Wangkheirakpam V D, Bhowmick B and Pukhrambam P D 2020 *IEEE Trans. Nanotechnology* **19** 156
[33] Kanungo S, Chattopadhyay S, Gupta P S, Sinha K and Rahaman H 2016 *IEEE Trans. Electron. Devices* **63** 2589
[34] Verma M, Tirkey S, Yadav S, Sharma D and Yadav D S 2017 *IEEE Trans. Electron. Devices* **64** 3841
[35] Goswami R and Bhowmick B 2019 *IEEE Sens. J.* **9** 9600